Elsevier Editorial System(tm) for Journal of Atmospheric and Solar-Terrestrial Physics
Manuscript Draft

Manuscript Number:

Title: The Equatorial and Low Latitude Ionosphere Within the Context of Global Modeling

Article Type: Special Issue:Ionosph/Thermosph-MKelley

Keywords: Ionospheric variability; General Circulation Modeling; Coupling of Atmospheric Regions; Equatorial Aeronomy; Low Latitude Ionosphere.

Corresponding Author: Miss Joei Wroten, B.S.

Corresponding Author's Institution: Boston University

First Author: Michael Mendillo, Ph.D.

Order of Authors: Michael Mendillo, Ph.D.; Joei Wroten, B.S.; Raymond Roble, Ph.D.; Henry Rishbeth, Ph.D.

Abstract: The Thermosphere-Ionosphere-Mesosphere-Electrodynamics Coupled Model TIME-GCM, coupled to the NCEP lower atmosphere model, is used to simulate the noontime ionospheric peak electron density NmF2 at low latitudes for the year 2002. The modeled NmF2 at Ascension Island and Darwin matches the general trend of the data fairly well throughout the year, but at Jicamarca it is about double the observed NmF2, so the equatorial trough is shallower in the model than actually observed. At all sites the actual day-to-day variability of NmF2 is about twice the modeled variability, possibly because of influences at lower heights in the atmosphere.

Manuscript
Click here to download Manuscript: wroten_LowLat_Apr22.doc
Click here to view linked References

The Equatorial and Low Latitude Ionosphere Within the Context of Global Modeling

Michael Mendillo[a], Joei Wroten[a,*], Raymond Roble[b] and Henry Rishbeth[(c,a)]

[a] Center for Space Physics, Boston University, Boston, MA 02215 USA

[b] High Altitude Observatory, National Center for Atmospheric Research, Boulder, CO 80307 US

[c] School of Physics and Astronomy, University of Southampton, Southampton, SO17 1BJ, UK

mendillo@bu.edu, jwroten@bu.edu, roble@hao.ucar.edu, hr@phys.soton.ac.uk

Abstract: The Thermosphere-Ionosphere-Mesosphere-Electrodynamics Coupled Model TIME-GCM, coupled to the NCEP lower atmosphere model, is used to simulate the noontime ionospheric peak electron density NmF2 at low latitudes for the year 2002. The modeled NmF2 at Ascension Island and Darwin matches the general trend of the data fairly well throughout the year, but at Jicamarca it is about double the observed NmF2, so the equatorial trough is shallower in the model than actually observed. At all sites the actual day-to-day variability of NmF2 is about twice the modeled variability, possibly because of influences at lower heights in the atmosphere.

* Corresponding Author. Center for Space Physics, Boston University, 725 Commonwealth Avenue, Boston, MA 02215, U. S. A. Tel: +00-1-617-353-2631; fax: +00-1-617-353-6463; E-mail address: jwroten@bu.edu

Keywords: Ionospheric variability, General Circulation Modeling, Coupling of Atmospheric Regions, Equatorial Aeronomy, Low Latitude Ionosphere.

1. Introduction.

Historically, the study of the terrestrial ionosphere was most often done within the context of three latitude zones: high latitudes (auroral and polar cap), middle latitudes (equatorward of the trough, poleward of the Appleton Anomaly), equatorial and low latitudes (within the crests of the Appleton Anomaly, which is otherwise known as the equatorial ionization anomaly, EIA). Such distinctions are less relevant today as global models address the full upper atmospheric system with couplings between latitude zones, as well as to and from regions above (magnetosphere) and below (troposphere-stratosphere). All of the basic physical processes acting upon the ionosphere are now well understood, and thus the success of models depends upon correct simulation techniques for those processes and, of course, the accuracy of input parameters.

There are several ways to assess the results: (1) Do well-known morphology patterns in specific regions appear correctly in the results from global model? (2) Do the models reproduce observed day-to-day variability? (3) Do simulations of large disturbance effects, e.g., thermospheric-ionospheric storms, agree with observed case study events? To address item (3) in a comprehensive way, it is first required to validate the basic simulation capabilities of a model by addressing item (1). Day-to-day variability (2) is in many ways the most difficult to address since it includes both background morphology and variable sources of perturbations (but not always extreme ones). Having the correct blend of all processes on each day of a year is clearly the most challenging task for a true first principles global model.

The suite of models developed at the National Center for Atmospheric Research (NCAR) over the past decades offers the opportunity to address these issues via detailed comparisons of predictions with actual observations. First, using a set of ten representative ionosonde stations at mid-latitudes, values of the ionosphere's maximum electron density (NmF2) were studied using six years of data with moderate solar flux (1960, 1967, 1970, 1978, 1983 and 1988), for which the mean F10.7 was 144 units and mean Ap was 15 (Rishbeth and Mendillo, 2001). Then, the Thermosphere-Ionosphere-Mesosphere-Electrodynamical General Circulation Model (TIME-GCM) coupled with the lower atmosphere's Community Climate Model 3 (CCM-3) was run for a full year with constant solar and geomagnetic sources typified by F10.7 = 140 and Ap = 4. This enabled item (1) to be studied as a climatological process and item (2) to be studied using only variable sources from below (Mendillo et al., 2002). When compared to observations at six mid-latitude ionosonde stations, the results pointed to the important role of meridional winds, and to a lesser extent composition (O/N_2 ratio), as the dominant contributor to day-to-day variability. For stations such as Slough in the northern hemisphere and Port Stanley in the southern hemisphere, the observed monthly variability of 20% (daytime) and 40-60% (nighttime) were simulated as 10% (daytime) and 20-30% (nighttime) by the model. With variability only possible via day-to-day changes in solar zenith angle and coupling from below (solar and geomagnetic sources being constant for the full simulation year), the central conclusion reached was that total variability indeed has a significant contribution from non-solar and geomagnetic forcings. Future model development has thus been aimed at exploring alternate methods of portraying this upward coupling.

2. Model Characteristics and Data Sources

2.1 TIME-GCM-NCEP.

Roble (2000) described how the TIME-GCM was coupled to the CCM-3 in order to investigate how sources of variability generated in the troposphere and stratosphere propagate into the thermosphere and ionosphere. To investigate another method of coupling from the lower atmosphere, the TIME-GCM was subsequently adapted to flux-coupling from the National Center for Environmental Predictions (NCEP) model (Randel, 1992). NCEP provides forcings of geopotential height and temperature at the 10 hPa pressure level (about 28 km) every 24 hours. Zonal and meridional winds at this lower boundary set the planetary wave structure around the globe. Superimposed upon these are diurnal and semi-diurnal propagating tides derived from the Global Scale Wave Model (GSWM) of Hagan et al. (1999). When added to the thermosphere-ionosphere components, the TIME-GCM-NCEP spans heights from about 30 km to a top pressure level near 500 km.

For the upper atmosphere, all of the standard solar and geomagnetic inputs remained as before, as well as the grid spacing of 5° in latitude and longitude horizontally and 2 grid points per neutral scale height vertically, with time steps of 5 minutes. Rather than using a 'generic' year for the simulation, the TIME-GCM-NCEP model was run for the full year 2002. The model used as input the actual F10.7 daily index, with high latitude (auroral) input sources parameterized using the 3-hour geomagnetic index Kp. During the year F10.7 decreases from about 240 to 150 with several fluctuations, with an average for the year of 180 that is appropriate for a year of moderately high solar activity. The results from the 365-day run created a new set of global output parameters–an enormous amount of information to examine. Thus, the first step was to characterize performance at mid-latitudes using observed 2002 NmF2 data from the same set of ionosonde stations previously examined in Rishbeth and Mendillo (2001) and Mendillo et al. (2002). Encouraged by the results from this new study at mid-latitudes (Rishbeth et al., 2008), we now turn to the equatorial domain and, for this pilot study, limit our comparisons to three ionosonde stations.

2.2 Data Sources.

For our low latitude study, the three ionosonde stations chosen are based on two selection criteria: maximizing the availability of data for the full year, and their locations at different latitudes in different longitude zones. The selected stations are: Jicamarca, Peru (12^{o}S, 283^{o}E, −3^o geomagnetic latitude), Ascension Island in the Atlantic sector (8^{o}S, 346^{o}E, −10^o geomagnetic latitude), and Darwin, Australia (13^{o}S, 131^{o}E, −22^o

geomagnetic latitude). It so happens that all three stations are in the southern hemisphere but, given that geomagnetic latitude is the dominant influence in regions spanning the equatorial ionization anomaly, hemispheric differences and longitude variations should be of lesser importance, and thus we expect these sites to represent the geomagnetic equator, the equatorward flank of the EIA, and poleward of the EIA crest.

Figure 1 (a, b, c) show the observed behavior of NmF2 at each of these sites using hourly values, with panels divided by calendar month. All data are provided in UT and thus our analyses for different longitude sectors are also conducted in UT, but noon and midnight local time (LT) are marked on the time axis at the bottom of each figure. There are several diurnal and seasonal features to note from these plots. Starting with the equatorial site Jicamarca, Figure 1(a) shows that there are essentially two types of diurnal patterns. From January to April, there are three periods of local maxima: pre-noon, late-afternoon, and nighttime. This is particularly prominent in March and April, when the absolute values of NmF2 are the highest of the year. Then, from June to October, the diurnal pattern is more uniform during the daytime, followed by a nighttime secondary maximum, particularly clear in September and October. The absolute values of daytime NmF2 are clearly lower than in other months. May and November appear as transitions between these two basic patterns. That the March and October equinox periods are so different is perhaps not widely appreciated. We defer a discussion of the physical causes of these diurnal features to Sections 4 and 5, and continue here with morphologies from the other two stations, and then model results.

Ascension Island is near the southern crest of the EIA. As seen from Figure 1(b), data sets for January, April, September are too sparse to discuss. All other months show a very high degree of variability; e.g., compare July and October with Jicamarca data for those months in Figure 1(a). The pattern of three diurnal maxima found at Jicamarca is not consistently found in any month at Ascension Island. Rather, there is a daytime maximum and a subsequent secondary peak either near dusk, as in March, or during midnight hours, as in October, November and December. The absolute value of daytime NmF2 shows a mid-year minimum and equinoctial maxima.

In Figure 1 (c), the data from Darwin refer to a location typically poleward of the EIA. From January to April, there are two diurnal maxima, before and after noon. In subsequent months (with data), the diurnal pattern is one of steady decline from the pre-noon maximum. For absolute values, daytime NmF2 data are at their minima in June and July, with again evidence for equinoctial maxima. There are some obviously unusual days in the Darwin data, probably ionospheric storms that are more pronounced at lower mid-latitudes than at sites closer to the geomagnetic equator (Mendillo, 2006).

3. Simulation Results.

3.1 Model Comparisons: Diurnal Patterns, Absolute Magnitudes and Day-to-Day Variability.

The TIME-GCM-NCEP model output was extracted from the grid points closest to the three stations, and hourly values were used for comparisons with Figure 1. To facilitate such comparisons visually, we use the format developed in Mendillo et al. (2002) in which the observed monthly means ±1 standard deviation σ are shown as a shaded diurnal pattern for each month, with the daily curves from the model superimposed. Inspection of Figure 2 (a, b, c) provides a quick way to assess how the model results compare in diurnal shapes, absolute magnitudes and variability levels throughout the year.

Again taking the stations in order of progression away from the geomagnetic equator, we see that at Jicamarca the overall diurnal patterns from the model in Figure 2(a) are all relatively similar for each month of the year. There is a single daytime maximum followed by a nighttime secondary peak in all months but January and December. The absolute values are in good agreement during nighttime hours for most of the months. The daytime values are acceptable early and late in the year, with model values about a factor of two too high from June to October. When all or most of the model's diurnal curves fall within the red shading (e.g., in February and November), then the variability is well below observations (recall that the shading is ±1σ and thus should include only about two-thirds of the daily values, not all of them). In some months, e.g., July and October, the model variability exceeds the variability in the data

At Darwin, Figure 2(b) shows diurnal curves that are again similar in shape in all months. The second diurnal peak shown in the data (shading) is missing rather dramatically in the January-April comparisons, though there is a hint of increased variability during those post-sunset hours, indicating some changing physical conditions, possibly dynamical, in addition to simple photochemical decay. Absolute values of daytime NmF2 are rather good in some months (e.g., January-March, October), but excessively high in other months (e.g., June-September). Variability is pronounced in most months, and particularly so in April and July.

At Ascension Island, Figure 2 (c) again shows consistently-shaped diurnal curves in all months. The secondary maxima spanning dusk to midnight that occur in the data from January to March and October to December are not captured in the model. Absolute values of NmF2 are, on average, quite good in comparisons to the data over the full year. Variability is pronounced in the model for each month, ranging from minimal day-to-day differences in March and December, to patterns more comparable to data in other months. We defer discussion of these patterns to Section 5.

3.2 Model Comparisons: Annual Patterns at Noon

To take advantage of the full capabilities of a General Circulation Model, we now examine mid-day behavior of observed NmF2 within the context of model output for NmF2, the photochemical O/N_2 concentration ratio, and the dynamical parameters of meridional neutral winds (U_n) and vertical plasma drift (V_z), with the latter three taken at the hmF2 pressure level where NmF2 occurs. Figure 3 (a) gives the results for Jicamarca. In the top panel, the noontime values from observations (solid dots) and the model (open dots) are shown for each day of the year. The semi-annual pattern of equinoctial maxima is apparent in both, with the effect somewhat over-represented in the model. The main cause of this predominantly photochemical effect upon both absolute magnitudes and seasonal patterns is the O/N_2 ratio shown in the second panel. For most of the year, there is proportionally more atomic oxygen in the model (ratios > 15) and thus photo-production has exaggerated effects. The third panel shows the meridional neutral wind which, at this latitude, is geomagnetically trans-equatorial. The pattern over the year is one of poleward winds associated with lower NmF2 in the Jan and June-July solstice months, but not in the December period. The wind speeds are not large, and thus the transport they drive may not be as dominant to local NmF2 values as plasma dynamics. The final panel gives vertical plasma drift, showing all noontime values within a factor of two (10-20 m/s) throughout the year, corresponding to eastward electric fields of 0.25-0.5 mV/m. The annual pattern of NmF2 in the model thus depends upon these three important processes, and each shows considerable variability in absolute magnitude over the course of a full year.

Turning now to Ascension Island, Figure 3(b) presents the same analysis. In the top panel, data and model are in excellent agreement at noon, both in magnitudes and in a semi-annual pattern that includes considerable small scale structure. The O/N_2 ratio in the second panel exhibits a rather limited range (values of 5-10) that allow photochemistry to yield correct NmF2 values over the course of the year. The neutral winds in the third panel are poleward for the full year, with strongest winds at mid-year moving plasma to lower altitudes and thus enhancing the loss, resulting in the smallest noontime peak densities shown in the top panel. Finally, the vertical E x B drift varies by a factor of three (values of 5-15 m/s), providing yet another source of variability.

The Darwin results in Figure 3(c) show excellent agreement for noon values, with a clear semi-annual pattern of well-matched absolute values of NmF2 during the first half of the year, and somewhat less consistent agreement after the June solstice (with missing data late in the year). In the second panel, the O/N_2 ratios between 5 and 10 result in model values for NmF2 consistent with observations, though somewhat too high between mid-year and the September equinox. Meridional neutral winds (U_n) have an annual pattern with peak poleward magnitudes at the time of the annual minimum in NmF2 (June solstice). The electrodynamic vertical drift has a noticeably annual pattern, in contrast to the other sites closer to the equator, with smallest drifts at the times of the annual minimum in NmF2. The variability of V_z spans a factor of two (10-20 m/s), similar to that found at Jicamarca.

3.3 Model Comparisons: Geomagnetically Quiet vs. Disturbed Days.

Current day research on the response of the ionosphere to increases in geomagnetic activity most often deals with "case studies" of individual storm periods. At mid-latitudes, there is a short but dramatic positive phase in F-layer densities and total electron content (TEC), followed by one to several days of depletion (negative phase) effects. For the equatorial and low latitude region, there is often a brief initial phase related to the sudden growth of the equatorial ionization anomaly (EIA), producing negative and positive effects at the equator and EIA latitudes, respectively. Then, a period of one or more days of enhanced densities (positive phase) occurs (Prölss, 1995).

In a recent review of TEC storm effects at all latitudes (Mendillo, 2006), emphasis was placed on the statistical results that come from the analysis of many ionospheric storms. The dominant "characteristic patterns" associated with geomagnetic activity (in terms of the number of days affected) is thus the negative phase at mid-latitudes and the positive phase at low latitudes. Changes of thermospheric composition and circulation, initiated by storm-time input at auroral latitudes, are a well-accepted explanation of these delayed-effect morphologies (Prölss, 1995; Rishbeth, 1975). NCAR General Circulation Models have been successfully used to understand observed case study results (e.g., Lu et al., 1998). While large storms occurred in 2002, here we confine our investigation to examining how daily changes in geomagnetic activity input manifests itself at equatorial and low latitudes and, in particular, contributes to day-to-day variability within each month.

Figure 4 summarizes the solar and geomagnetic activity variations that occurred in 2002. This is a somewhat typical pattern for a year following solar maximum, with a modest decline in solar irradiance (as shown by the proxy F10.7 index), and a semi-annual variation in geomagnetic activity (as shown by the Ap index). We first investigate how the variability in geomagnetic activity might relate to the observed and modeled variability at the three ionosonde stations. To summarize this over a full year, we turn to the "parameter quilts" format used in our earlier study of mid-latitude data-model comparisons (Mendillo et al, 2002). Figure 5 portrays the year 2002 in 33 segments of 11-days, with a single color bar used to relate changes in several key parameters. For example, the top row gives the 11-day averages of Ap (in its units), with the second row giving the $\pm 1\sigma$ standard deviation (in percentage) about that 11-day Ap mean. Thus, the semi-annual pattern of Ap is shown by the green color bar values (typical of Ap = 25 units) for segments within equinox months; these segments also have higher Ap variabilities, as shown in the second row. Next, the observed variability of NmF2 (σ, %) of the 11-day means are given from the three sites: Jicamarca (J), Ascension Island (AI) and Darwin (D). At the magnetic equator, there is no correlation between the high levels of observed variability and geomagnetic activity, and the same appears to be the case at Ascension Island (though there are several periods of missing data). At Darwin, there is a variability correlation during the segment of highest Ap (in April), but the subsequent equinox has low variability when σ(Ap, %) of is still relatively high.

In the second and third panels, results from the model's output for variability of NmF2 and the O/N_2 ratio are also analyzed in the same 11-day segments at each of the three sites, with results portrayed in the same quilt format. The top two rows repeat the Ap and σ(Ap, %) to facilitate comparisons. Several impressions appear from a visual inspection: (a) The model produced more variability at the geomagnetic equator than at the low latitude sites, (b) there is no clear relationship of this variability to changes in geomagnetic activity, and (c) the model's σ(NmF2, %) at all three stations are uniformly lower than observed σ(NmF2, %) in the top panel (e.g., the color codings at AI and D are dominated by blue shades (10%) corresponding to about half of the observed variability).

In the bottom panel, the same format is used for the O/N_2 ratio from the model. Visual inspection suggests (a) that variability levels of composition change are comparable to those of NmF2, (b) that O/N_2 variability is highest at the highest latitude (Darwin), and (c) at Darwin, the variability in composition seems to be related to the variability in Ap. We conclude that the TIME-GCM-NCEP produces ionospheric F-layer variability from its simulated changes in neutral composition, but that the effects are relatively small near the magnetic equator, but increase towards mid-latitudes.

Another way to assess the effects of geomagnetic activity is illustrated in Figures 6 and 7. Here we select the active month April 2002, with a monthly mean $\langle Ap \rangle_{MM} = 15$ and $\sigma(Ap) = \pm 20\%$, and with relatively high variability due to daily values ranging from 2 to 70 Ap units. The 5 days of lowest magnetic activity had $\langle Ap \rangle_{QQ} = 3$ and the 5 days of highest activity had $\langle Ap \rangle_{DD} = 57$. We use the equatorial station Jicamarca for sample results since it has been studied for many decades both observationally and via modeling. In Figure 7 (top left panel), the diurnal curves observed on the 5 QQ days are shown by green dotted lines and the corresponding days from the model are shown by green solid lines. In the right panel, the same format is used for the 5 DD days, with orange dotted lines for observations and solid orange lines for model output. The observations show that the DD days have somewhat higher values than the QQ days, consistent with the statistical storm patterns discussed above. The model shows very little difference in absolute values between QQ and DD days, with a slight tendency for the quiet values being higher than the disturbed values. As noted earlier, the daytime shapes of the diurnal curves from the model differ significantly from observations, a trend not dependent upon geomagnetic activity. For both data and model, the variability of the DD days is slightly higher than that for the QQ days (and mostly at night). Taken together, observations and model results confirm the impression that geomagnetic activity is not a major driver for statistical variability at the geomagnetic equator.

In the lower panels, we portray model output for the O/N_2 ratio, meridional winds, and vertical plasma drift. The color coding is the same as in the upper panels, i.e., the 5 QQ days are shown in green and the 5 DD days are shown in orange, with the remainders in solid black lines. One can see some interesting patterns. First of all, there is a clear difference in the O/N_2 ratio on QQ vs. DD days (in comparison to the monthly means, given by the shading), but the lower values occur during QQ days when the model gives higher NmF2 values. The meridional winds (third panel) and vertical plasma drifts (fourth panel) also show separation of QQ patterns from DD patterns in the model.

Given that the overall diurnal curves in the top panel do not differ appreciably between QQ vs. DD days, particularly during daytime hours, we conclude that the three factors (a) photochemistry determined by O/N_2, (b) meridional transport driven by north-south winds, and (c) vertical changes in fountain effect processes driven by vertical plasma drift tend to combine to produce only minor changes in NmF2 for QQ vs. DD days.

4 Comparisons with Previous Models.

4.1. Empirical Models.

The morphology of the equatorial and low latitude ionosphere was, of course, one of the most intriguing "anomalies" studied during the discovery era in ionospheric physics (see summary in Rishbeth and Garriott, 1969). Comprehensive modeling work was conducted by Anderson (1973a,b; 1981) and others, and a basic understanding of the region's climatology was achieved, namely, that photochemical process were significantly affected by the unique electrodynamics and neutral wind patterns at low latitudes. Lee and Reinisch (2006) and Lee et al. (2008) have recently compared ionosonde observations from Jicamarca during high and low solar flux years, respectively, with predictions from the empirical International Reference Ionosphere IRI-2001 model (Bilitza, 2001, 2003). They review the past context of such comparisons as conducted, for example, by Adeniyi and Adimula (1995) and Adeniyi (2003) using ionosondes near the geomagnetic equator in Africa, and by Obrou et al. (2003), Batista and Abdu (2004) and Abdu et al. (2004) using ionosondes in Brazil. In all cases, there was an acceptable level of agreement between the F-layer's maximum density (NmF2), averaged to form monthly mean diurnal curves, from IRI and observations. Of relevance to our studies at Jicamarca, Lee and Reinisch (2006) and Lee et al. (2008) used hourly values from only geomagnetically quiet days ($\Sigma Kp \leq 24$) to form monthly mean values for two 12-month periods: 1996 (solar minimum, <F10.7> = 72) and April 1999-March 2000 (solar maximum, <F10.7> = 165). Our study for 2002 with <F10.7> = 180 units is thus for a comparable solar maximum period. Given that IRI is derived from observations, the shapes and magnitudes of the diurnal curves at Jicamarca capture the quiet-time diurnal patterns rather successfully. For TIME-GCM-NCEP, with all days of a month in the simulations and data comparisons, the first-principle calculations shown in Figure 2 for Jicamarca have somewhat mixed results, agreeing more in average absolute values than in diurnal shapes. We now discuss this further.

4.2. First Principles Models.

Several years ago, the NCAR Thermosphere-Ionosphere-Electrodynamic General Circulation Model (TIE-GCM) was run for a series of solar cycle conditions (minimum, medium, maximum) for equinox and solstice periods. When assessed using global mean parameters in the F2-layer (Fesen et al., 2002), the TIE-GCM's neutral temperature was found to be within 10% of MSIS values (with a tendency for the model to be higher), while the atomic oxygen mixing ratios exceeded those in MSIS by up to 20%. Global mean electron densities from TIE-GCM, when compared to IRI, were low by up to 50% for December solstice at solar minimum, but by less than 20% at solar maximum.

Upon this background, Fesen et al. (2002) then focused on the first model/data comparisons at equatorial and low latitudes using a set of data taken in and around Jicamarca during the months of October in 1996 and 1997 (solar minimum years). Fesen et al. (2000) had previously achieved success with the TIE-GCM in simulations of the pre-reversal enhancement (PRE) in the equatorial vertical plasma drift, one of the major drivers of morphology patterns at low latitudes, but it is the Fesen et al. (2002) study that compared F2-layer predictions with observations. For the fundamental ionospheric parameter of interest here, NmF2, the TIE-GCM values during daytime hours were smaller than observed values by up to 40%, and even this level of agreement was only possible if the O^+ downward fluxes in the model were kept downward at all local times. This unrealistic condition probably addressed shortfalls in a variety of processes not adequately represented by boundary conditions at the lower level (100 km in TIE-GCM), e.g., tidal modes and electron densities necessary to produce sufficiently large upward plasma drifts in the pre-noon hours. Fesen et al. (2000) had shown that for successful PRE simulations, the electron density in the E-layer has to be rather small, i.e., NmE = 1.5×10^3 e^-/cm^3.

In a later study of optical emissions from the thermosphere that used the same TIE-GCM output described in Fesen et al. (2002), Colerico et al. (2006) found that airglow signatures from the relaxation of the PRE lagged observations by up to 1.5 hours. That is, the observed morphology of the 6300Å inter-tropical arcs due to the relaxation of the fountain effect occurred noticeably earlier in the model.

As a second test case, Colerico et al. (2006) examined the transient airglow pattern (called a *brightness wave*) attributed to thermospheric dynamics arising from the midnight temperature maximum (MTM). They found that airglow generated from TIE-GCM output simply did not produce a brightness wave. The reason was traced to the fact that the MTM was barely 30^{o} K in the model (at 0300 LT), while observations showed it to be nearly a 200^{o} K enhancement at 0030 LT. Thus, winds (both meridional and zonal) from the MTM pressure bulge were essentially missing from the model. The overall conclusion reached from these three studies (Fesen et al., 2000, 2002; Colerico et al., 2006) was that while most morphology patterns found in data were also produced in the TIE-GCM, the local time phasing and magnitudes of crucial processes (winds and vertical drifts) were in need of remedy.

Meriwether et al. (2008) have presented the most recent study comparing observed MTM characteristics with a new version of the TIEGCM (one that includes terdiurnal tides forced by the non-linear interaction of the diurnal and semidiurnal tides). The model again failed to achieve agreement with thermospheric data, and thus the full representation of altitude/latitude coupling processes within a GCM remains as a major challenge.

In the present study, the new TIME-GCM-NCEP model being assessed includes the same physics from the TIE-GCM for the thermosphere and ionosphere, but has a very different set of conditions at a much lower simulation boundary (30 km). As shown in Figures 2-4 and in Tables 1-3, the TIME-GCM-NCEP absolute values have similar levels of success and failure (±50%) as found in the earlier TIE-GCM runs for average seasonal conditions at Jicamarca. Of importance is that shortfalls in absolute magnitude from TIE-GCM are now generally replaced by over-estimates in TIME-GCM-NCEP. The major contribution emerging from the newer model is therefore a new way to approach the topic of day-to-day variability, shown here for the first time at equatorial and low latitudes.

5 Discussion.

5.1 Diurnal Patterns.

The presence of the geomagnetic field at low latitudes, with a latitude dependence changing from completely horizontal at the equator (maximizing E x B vertical drift) to increasing inclination angles away from the equator (enhancing the effect of horizontal winds), makes the issue of absolute values of NmF2 more complicated than the standard compositional (O/N_2 ratio) control of photochemical processes. That is, over the latitude span of the EIA, neutral winds and plasma drifts modulate photochemical production and loss rates via redistributions of plasmas with respect to neutrals. Moreover, there can be dramatic advection effects of the strong spatial gradients often present. Thus, given the sensitivity to coupled processes, it is to be expected that minor shortfalls in winds and electric fields generated self-consistently within a GCM result in appreciable differences in the absolute magnitudes of NmF2 values when compared to observations. When judged by monthly mean values (observed vs. modeled), the agreement is rather impressive (see Table 1 for daytime and nighttime averages).

The characteristic diurnal patterns from observations and models offer opportunities to address more fundamental concerns. When discussing the observations in Figure 1, we pointed to the "three diurnal maxima" that appear during several months at various locations. While that is a reasonable way to describe such a pattern, the physics driving such features at the equator involves only two time periods. As summarized nicely in Lee and Reinisch (2006) for Jicamarca's location, there is a "mid-day-biteout" that causes the apparent independent appearance of a pre-noon peak and an afternoon peak. This is a consequence of the daytime "fountain effect" driven by vertical plasma drift at the magnetic equator and neutrals winds blowing away from the equator at noon (Rajaram and Rastogi, 1977). At dusk, the pre-reversal enhancement (PRE) again moves plasma upward at the equator, with higher speeds than at noon, and the resulting effect upon the observed F-layer is another "bite-out" that recovers to an apparent 3rd maxima later in the night. Thus, two episodes of dynamical effects account for the three diurnal structures seen at the equator. At a site off the geomagnetic equator (such as Ascension Island), observations do not show a dramatic transport effect from the mid-day-biteout, but certainly a most pronounced one from the PRE-induced dynamics.

Such latitude-coupled morphologies have been addressed comprehensively in modeling work by Anderson and Klobuchar (1983) for Ascension Island using a month of total electron content (TEC) data in September 1979. The results of that work showed that the post-noon decrease in F-layer densities results from both regular chemical decay augmented by downward motions driven by both meridional (poleward) and zonal (eastward) neutral winds. At Ascension Island, where the geomagnetic declination is substantial, the zonal winds play a more prominent role than would be expected at other longitudes, and thus the primary mechanism identified by Anderson and Klobuchar (1982) is the important role of the onset of strong poleward winds after 1400 LT in hastening chemical loss. When the electrodynamic "pre-reversal enhancement" of vertical drifts sets in near sunset, this upward motion at 1800-2000 LT accounts for the "secondary maxima" via a combination of reduced loss and advection. The monthly mean observations in Figure 2 show this second mechanism to be the main cause of diurnal structure at Ascension Island. Particularly good examples of coupled NmF2 patterns at and off the magnetic equator can be seen in March 2002 in Figures 2 (a) and (b).

The successful modeling of the Ascension Island observations by Anderson and Klobuchar (1983) was not by a self-consistent model, but one using three independent models for input conditions. These were: (a) an early version of the MSIS model for the neutral atmosphere (Hedin et al., 1977), (b) a representation of the vertical plasma drift measured at the Jicamarca by Woodman (1970), and (c) a composite model for winds taken from theory (Mayr et al., 1979) and observations at Kwajalein (Sipler and Biondi, 1978; Sipler et al., 1983). Thus, each of the two key dynamical parameters (winds and E-fields) could be tuned independently to show via computer simulations the types of background conditions needed to reproduce observations. For the TIME-GCM, however, far less flexibility exists. Some reassessments nevertheless need to be done. For example, as shown in Figure 6 in the simulations for April 2002, the plasma drifts at dusk (PRE) are comparable (about 30 m/s) to those used by Anderson and Klobuchar (1983), but the noontime values from the TIME-GCM (7 m/s) are a factor of 3 smaller. The meridional winds in Anderson and Klobuchar (1983) switch from equatorward to poleward at noon, and reach maximum values of 60 m/s at sunset, while in TIME-GCM the meridional winds in Figure 6 (for April) have that pattern earlier, i.e., from sunrise to noon and at somewhat smaller speeds.

5.2 Variabilities.

The observed monthly variability of midday and midnight NmF2 values at Jicamarca, Ascension Island and Darwin are shown graphically in Figure 2 and numerically in Tables 1, 2 and 3. The sample average results are ±22% daytime and ±33% nighttime. These are comparable to the daytime/nighttime results (±18% and ±29%, respectively) obtained for the equatorial stations Huancayo and Djibouti (both at 2^{o}N geomagnetic latitude) and the ±17% and ±40% at Vanimo (-11^{o} geomagnetic latitude) in Rishbeth and Mendillo (2001). Thus, the selection of stations for this study did not introduce any unusual observational results for day-to-day variability effects.

For the model results, the day vs. night monthly variabilities are ±7% (day) and ±20% (night) at the equator (Jicamarca), ±7% (day) and ±15% (night) at an EIA crest

(Ascension Island), and ±10% (day) and ±18% (night) poleward of the EIA (Darwin). Thus, with all sources of variability from above (solar and geomagnetic) and below (meteorological) included in the TIME-GCM-NCEP run for 2002, the overall variability in the model is well below what is observed. For midday, the model predicts a third to half the observed variability, while at night it improves to nearly two-thirds of the observed variability.

When examined in terms of the 5 most quiet geomagnetic days versus the 5 most disturbed days (Figure 7), significant changes in variability did not occur during daytime in either data or model), while both showed some increases at night. The overall impression is that this first assessment of F-layer variability produced by daily runs of a first-principles GCM is most encouraging at low latitudes. There are day-to-day differences throughout each month at each of the stations. Yet, the model again produces less variability than found in observations, at times by factors of 2 or 3, when judged by standard deviations about a monthly mean. As auroral input sources do not dominate the effects at low latitudes, we suggest that yet more work is needed on specifying coupling from below.

6. Summary and Conclusions.

This paper reports the first detailed modeling of the low latitude F2 layer with the Thermosphere-Ionosphere-Mesosphere-Electrodynamics Coupled Model TIME-GCM, coupled to the NCEP lower atmosphere model. The modeled noontime NmF2 at

Ascension Island and Darwin for the year 2002 matches the general trend of the data fairly well throughout the year. However, the modeled NmF2 at Jicamarca (2 degrees from the magnetic equator) is about double the observed NmF2, so the equatorial trough is shallower in the model than is actually observed. In the equatorial zone, the model results depend heavily on the neutral wind and electric field patterns, which are calculated self-consistently, and these require that conditions at lower altitudes are represented correctly. Thus, the detailed model versus data comparisons of the seasonal and local-time variations of electron density (Section 3) do not really test the sophisticated dynamics and photochemistry incorporated in the TIME-GCM.

Finally, for variability patterns, at all three sites the actual day-to-day variability of NmF2 is noticeably greater than the modeled variability. Again, we suspect that this short fall arises because of an under portrayal of influences at lower heights in the atmosphere. This difficulty of accounting for observed variability is quite often encountered in ionospheric modeling.

Acknowledgements.

We are most grateful to Ben Foster at NCAR for his assistance with the TIME-GCM-NCEP calculations and for providing model output for comparisons with ionosonde stations. We thank the World Data Centres A and C1 for Solar-Terrestrial Physics in Boulder (CO) and in Chilton (UK) for making ionosonde data available for studies such as this. The work at Boston University was supported, in part, by a grant from the Aeronomy Program of the US National Science Foundation (NSF). The NCAR modeling efforts are supported by grants from the NSF.

References

Abdu, M. A., Batista, I. S., Reinisch, B. W., Carrasco, A. J., 2004. Equatorial F-layer heights, evening prereversal electric field and night E-layer density in the American sector: IRI validation with observations. Advances in Space Research 34, 1953-1965.

Adeniyi, J. O., Adimula, I. A., 1995. Comparing the F2-layer model of IRI with observations at Ibadan. Advances in Space Research 15, 1441-1444.

Adeniyi, J. O., Bilitza, D., Radicella, S. M., Willoughby, A. A., 2003. Equatorial F2-peak parameters in the IRI model. Advances in Space Research 31, 507-512.

Anderson, D. N., 1973a. A theoretical study of the ionospheric F region equatorial anomaly, I. Theory. Planetary and Space Science 21, 409-419.

Anderson, D. N., 1973b. A theoretical study of the ionosphere F region equatorial anomaly, II. Results in the American and Asian sectors. Planetary and Space Science 21, 421-442.

Anderson, D. N., 1981. Modeling the ambient, low latitude R-region ionosphere ---A review. Journal of Atmospheric and Terrestrial Physics 43, 753-761.

Anderson, D. N., Klobuchar, J. A. 1983. Modeling the total electron content observations above Ascension Island. Journal of Geophysical Research 88, 8020-2024.

Batista, I. S., Abdu, M. A., 2004. Ionospheric variability at Brazilian low and equatorial latitudes: comparison between observations and IRI model. Advances in Space Research 34, 1894-1900.

Hagan, M. E., Burrage, M. D., Forbes, J. M., Hackney, J., Randel, W. J., Zhang, X., 1999. GSWM-98: Results from migrating solar tides, Journal of Geophysical Research 104(A4), 6813-6828.

Bilitza, D., 2001. International Reference Ionosphere 2000. Radio Science 36, 261-275.

Bilitza, D., 2003. International Reference Ionosphere 2000: examples of improvements and new features. Advances in Space Research 31, 757-767.

Colerico, M. J., Mendillo, M., Fesen, C. G., Meriwether, J., 2006. Comparative investigations of equatorial electrodynamics and low-to-mid latitude coupling of the thermosphere-ionosphere system. Annales Geophysicae 24, 503-513.

Fesen, C. G., Roble, R. G., Richmond, A. D., Crowley, G., Fejer, B. G., 2000. Simulations of the pre-reversal enhancement in the low-latitude vertical ion drift. Geophysical Research Letters 27, 1851-1854.

Fesen, C. G., Hysell, D. L., Meriwether, J. M., Mendillo, M., Fejer, B. G., Roble, R. G., Reinisch, B. W., Biondi, M. A., 2002. Modeling the low-latitude thermosphere and ionosphere. Journal of Atmospheric and Terrestrial Physics 64, 1337-1349.

Hedin, A. E., Reber, C. A, Newton, G. P., Spencer, N. W., Brinton, H. C., Mayr, H. G., Potter, W. E., 1977. A global thermospheric model based upon spectrometer and incoherent scatter data, MSIS. Journal of Geophysical Research 82, 2137-2156.

Lee, C.C., Reinisch, B. W., 2006. Quiet-condition hmF2, NmF2, and Bo variations at Jicamarca and comparison with IRI-2001 during solar maximum. Journal of Atmospheric and Terrestrial Physics 68, 2138-2146.

Lee, C. C., Reinisch, B. W., Su, S.-Y., Chen, W. S., 2008. Quiet-time variations of the F2-layer parameters at Jicamarca and comparison with the IRI-s001 during solar minimum. Journal of Atmospheric and Terrestrial Physics 70, 184-192.

Lu, G., Pi, X.-Q., Richmond, A. D., Roble, R. G., 1998. Variations of total electron content during geomagnetic disturbances: A model/data observation comparison. Geophysical Research Letters 25, 253-256.

Mendillo, M., 2006. Storms in the ionosphere: Patterns and processes for total electron content. Reviews of Geophysics 47, RG4001, doi:10.1029/2005RG000193.

Mendillo, M., Rishbeth, H., Roble, R., Wroten, J., 2002. Modelling F2-layer seasonal trends and day-to-day variability driven by coupling with the lower atmosphere. Journal of Atmospheric and Terrestrial Physics 64, 1911-1931.

Meriwether, J., Faivre, M., Fesen, C., Sherwood, P., Veliz, O., 2008. New results on equatorial thermospheric winds and the midnight temperature maximum, Annales Geophysicae 26, 447-466.

Obrou, O. K., Bilitza, D., Adeniyi, J. O., Radicella, S. M., 2003. Equatorial F2 layer peak height and correlation with vertical ion drift and M(3000)F2. Advances in Space Research 31, 513-520.

Prölss, G., 1995. Ionospheric F-region storms, in Handbook of Atmospheric Electrodynamics, vol. 2, edited by H. Volland, chap. 8, 195-248, CRC Press, Boca Raton, FL.

Randel, W. J., 1992. Global atmospheric circulation statistic, 1000-1 mb, NCAR Tech. Rpt 366, Boulder, Colorado.

Rishbeth, H., 1998. How the thermospheric circulation affects the ionospheric F2-layer, Journal of Atmospheric and Terrestrial Physics 60, 1385-1402.

Rishbeth, H., 1975. F-region storms and thermospheric circulation. Journal of Atmospheric and Terrestrial Physics 37, 1055-1064.

Rishbeth, H., Fuller-Rowell, T. J., Rees, D., 1987. Diffusive equilibrium and vertical motion in the thermosphere during a severe magnetic storm: a computational study. Planetary and Space Science 35, 1157-1165.

Rishbeth, H., Garriott, O. K., 1969. Introduction to Ionospheric Physics, Academic Press, New York.

Rishbeth, H., Mendillo, M, 2001. Patterns of F2-layer variability. Journal of Atmospheric and Terrestrial Physics 63, 1661-1680.

Rishbeth, H., Roble, R., Wroten, J., Mendillo, M., submitted 2008. Modelling the mid-latitude ionospheric F2-layer for year 2002 with the TIME-GCM coupled model. Journal of Atmospheric and Terrestrial Physics.

Roble, R. G., 2000. On the feasibility of developing a global atmospheric model extending from the ground to the exosphere, in Atmospheric Science Across the Stratopause, Geophysical Monograph 123, American Geophysical Union, 53-67.

Sipler, D. P., Biondi, M. A., 1978. Equatorial F region neutral winds from nightglow O I NM Doppler shifts. Geophysical Research Letters 5, 373-376.

Sipler, D. P., Biondi, M. A., Roble, R. G., 1983. F-region neutral winds and temperatures at equatorial latitudes: Measured and predicted behavior during geomagnetically quiet conditions. Planetary and Space Science 31, 53-66.

Woodman, R. F., 1970. Vertical drift velocities and east-west electric fields at the magnetic equator. Journal of Geophysical Research 31, 6249-6259, 1970.

Figure Captions

Figure 1. Observations of hourly values of NmF2 sorted by month for the year 2002 from three ionosonde stations: (a) Jicamarca (Peru), (b) Ascension Island (Atlantic Ocean) and (c) Darwin (Australia). All data are shown in universal time (UT), with markers on the lower axes showing local noon (open arrow) and local midnight (solid arrow).

Figure 2. TIME-GCM/NCEP model output for the three ionosonde sites shown in Figure 1 using the same format of hourly values in UT, with indicators for local noon and midnight. The shading in each panel gives the observed NmF2 monthly mean $\pm\sigma$ to aid in comparisons with Figure 1.

Figure 3. A comparison of noontime behavior of NmF2 from observations and model for the full year 2002 (top panel) at (a) Jicamarca, (b) Ascension Island, and (c) Darwin. In each figure, lower panels give model output at the height of maximum electron density of three parameters used in interpretation of results: the O/N_2 ratio, the meridional neutral wind (in m/s, positive equatorward), and vertical drift due to electric fields (in m/s, positive upward).

Figure 4. A summary of solar flux (using the F10.7 index) and planetary geomagnetic activity (using the daily index Ap) for the year 2002. Each point is a daily value.

Figure 5. 11-day segments of the year 2002 used to portray variability levels of geomagnetic activity, the ionosphere's NmF2, and the photochemical parameter O/N_2. In all three panels, the top two rows give the 11-day means for Ap and its standard deviation in percent over the full year. The top panel compares these $<Ap>_{11\text{-day}}$ and σ(Ap, %) with the observed 11-day noontime variability σ(NmF2, %) at three stations: J (Jicamarca), AI (Ascension Island) and D (Darwin). Using the same format, the second panel gives the model's results for noontime variability of NmF2, and the third panel gives the model's noontime variability of O/N_2. Note that the single color bar is used for units of $<Ap>_{11\text{-day}}$ and the standard deviations (in %) of the 11-day means of Ap, NmF2 and O/N_2.

Figure 6. For the month of April 2002, daily values of the geomagnetic index Ap are given, with the five most quiet days (QQ) and the five disturbed days (DD) indicated.

Figure 7. A comparison of ionospheric variability at Jicamarca using diurnal curves of several parameters for the 5 geomagnetic most quiet (QQ) and the 5 geomagnetic most disturbed (DD) days in the month of April 2002. The top panel (left) shows observed NmF2 (dotted green) curves and model NmF2 (solid green) curves for the QQ days. The right panel gives the observed (orange dotted) curves and the model (solid orange) curves for the DD days. The lower three panels use the same color coding to portray the QQ and DD patterns for the parameters O/N_2, meridional neutral winds (U_n) and vertical ExB drift (V_z). The shadings give the monthly mean ± 1σ (standard deviation) from the model output of the month.

Figure1--tiff format

Click here to download high resolution image

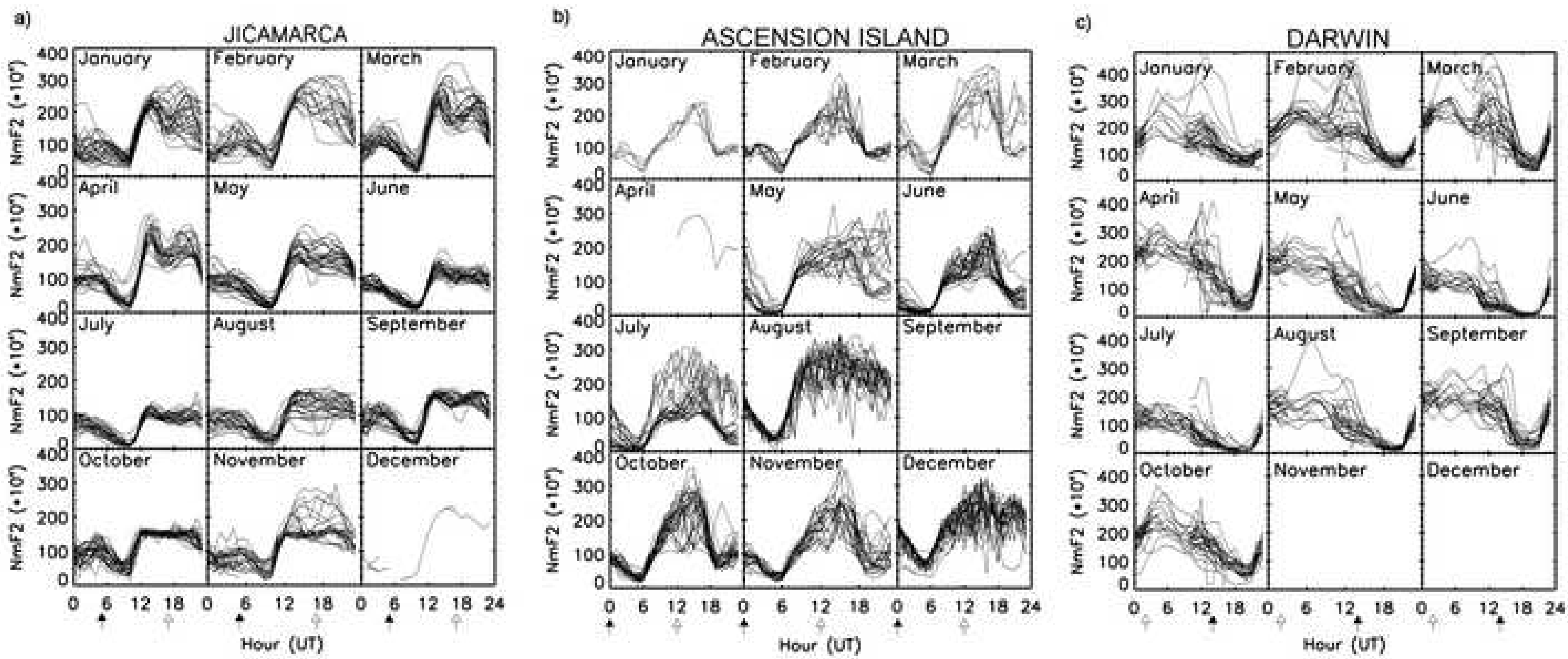

Figure2--tiff format

Click here to download high resolution image

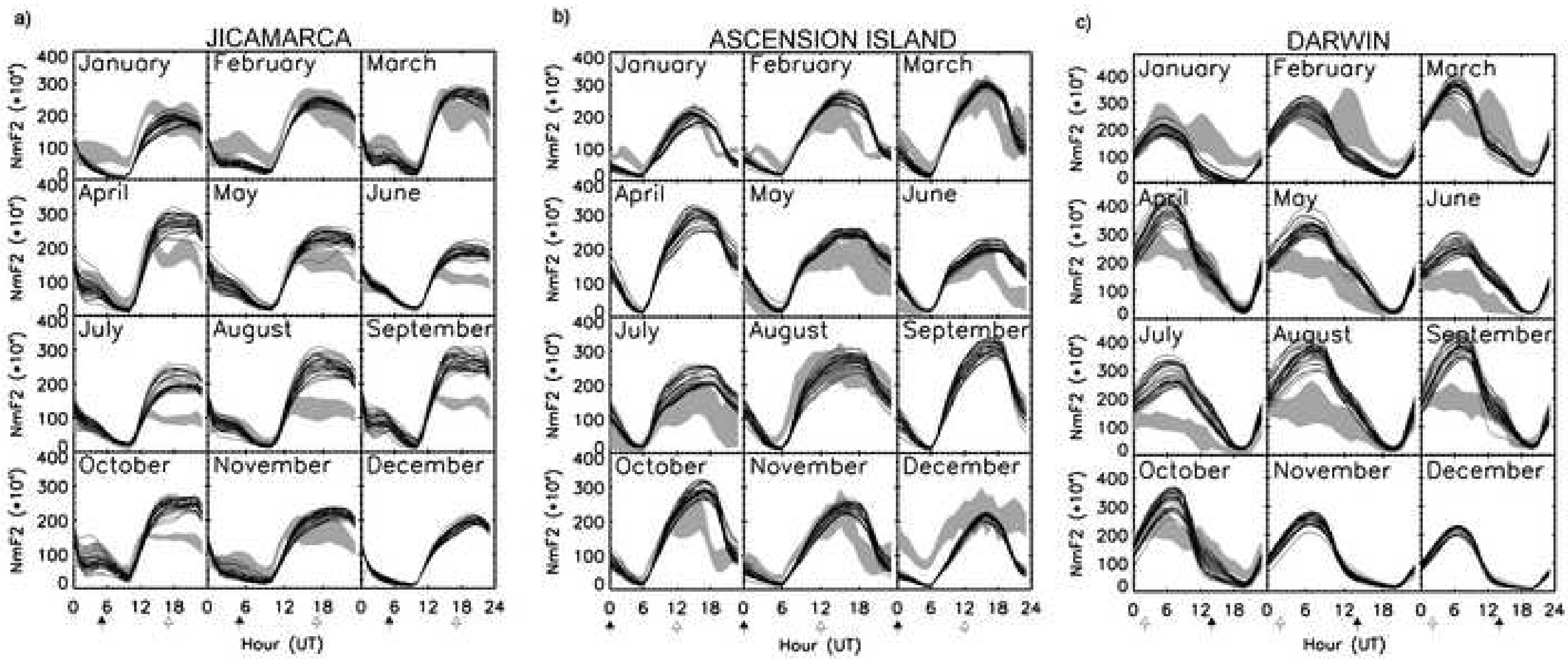

Figure3--tiff format

Click here to download high resolution image

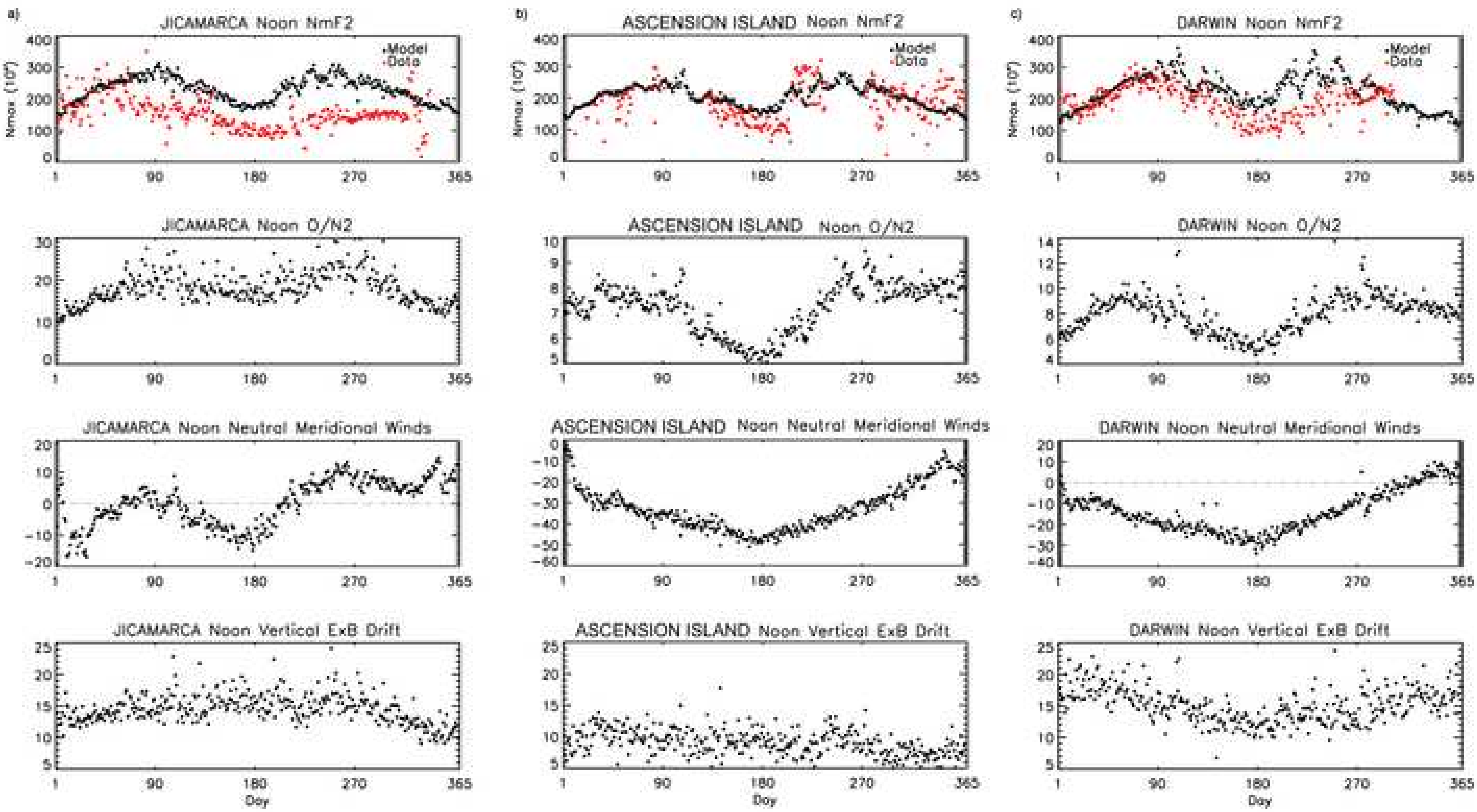

Figure4--tiff format

Click here to download high resolution image

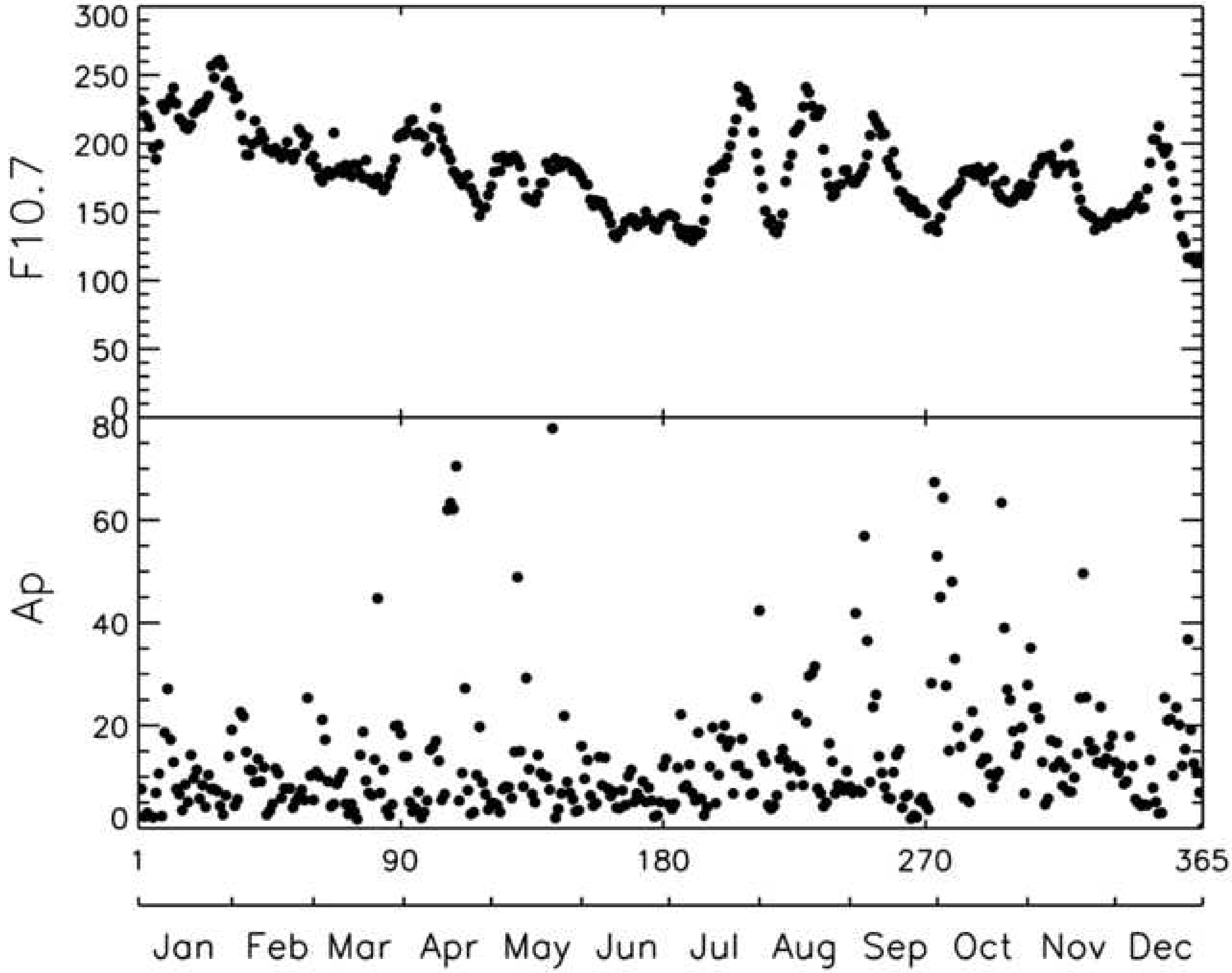

Figure5--tiff format
Click here to download high resolution image

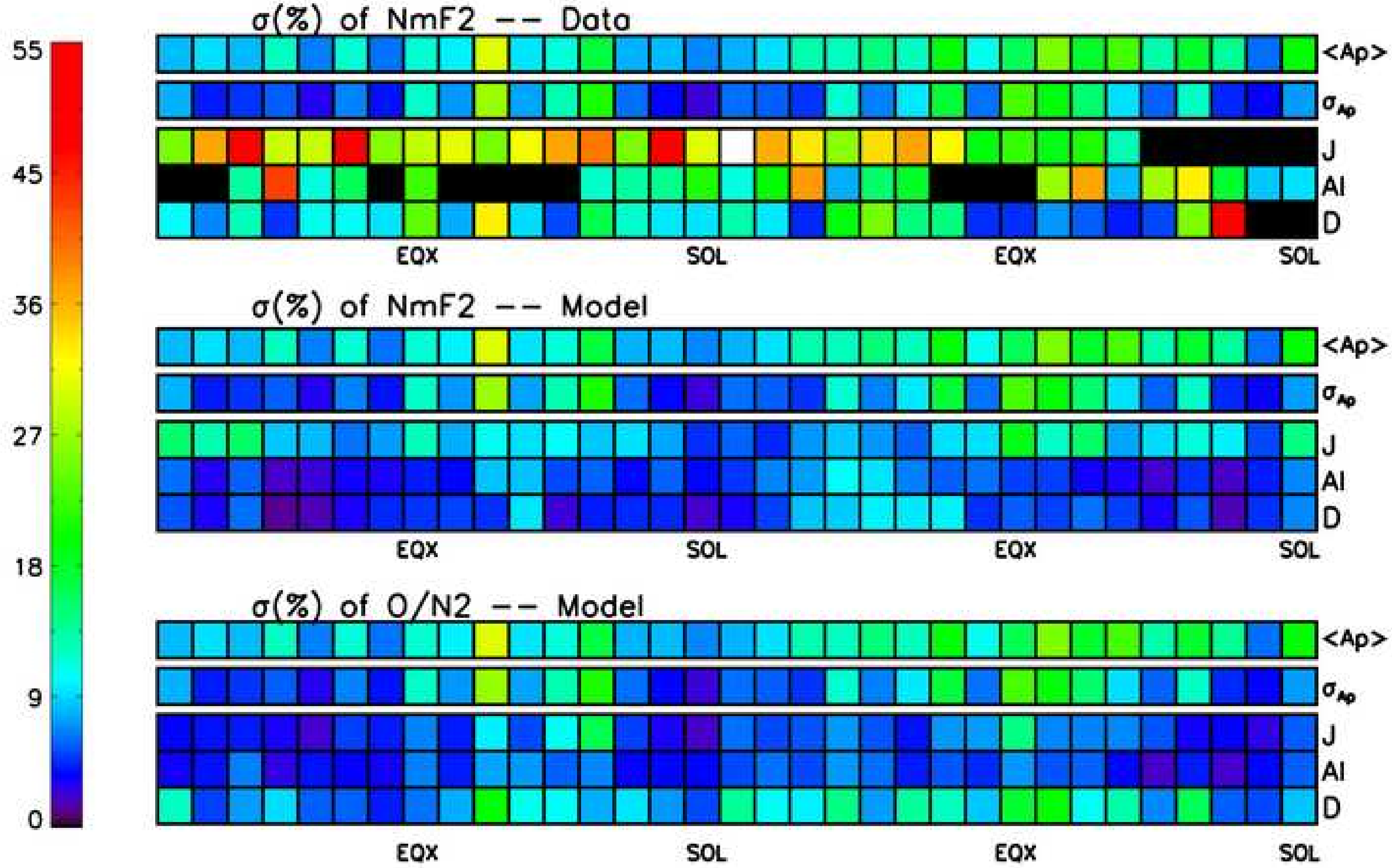

Figure6--tiff format
Click here to download high resolution image

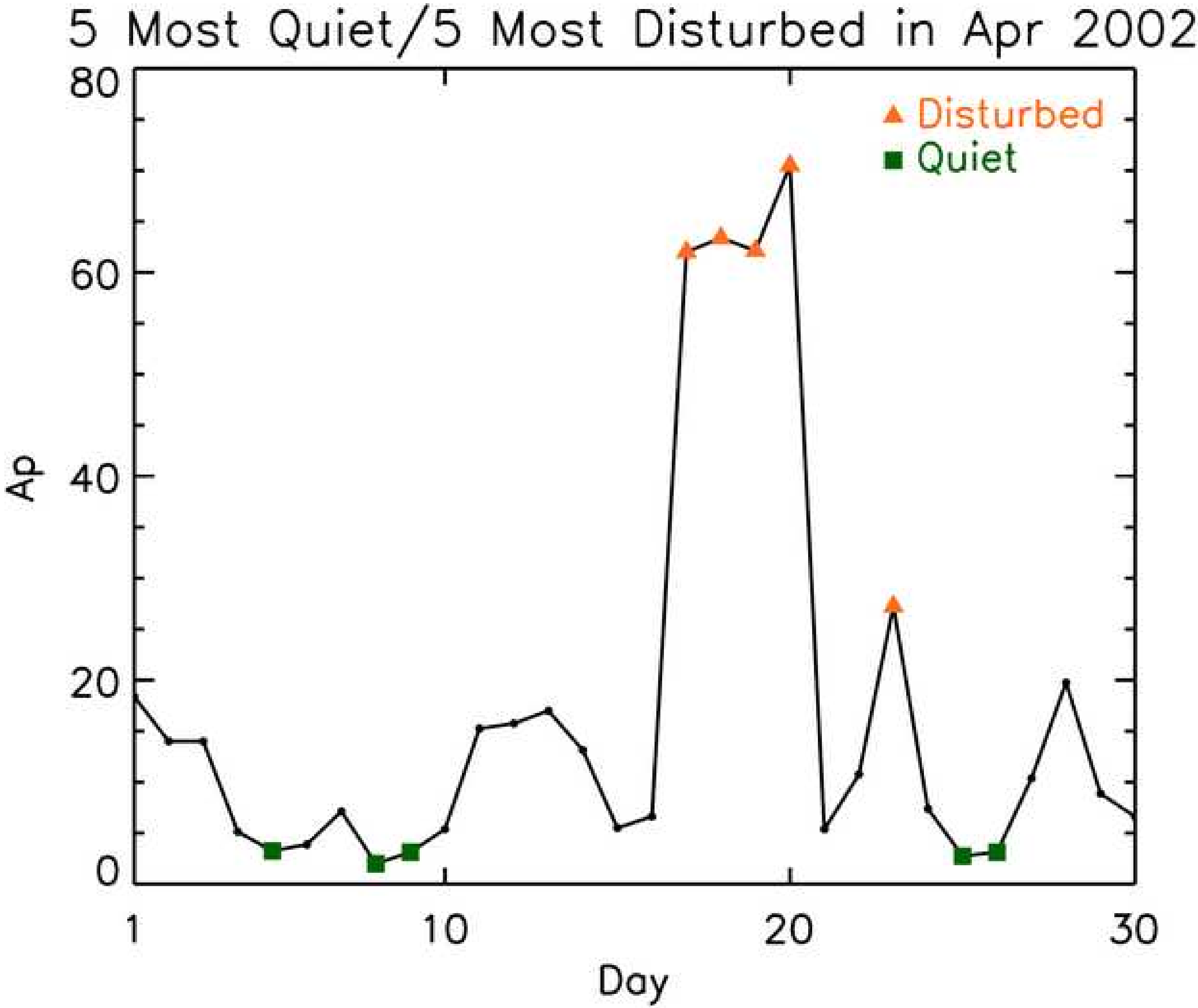

Figure7--tiff format

Click here to download high resolution image